Graphical abstract

Fabrication of novel Si-doped hydroxyapatite/gelatine scaffolds by rapid prototyping for drug delivery and bone regeneration pp xxx–xxx

F.J. Martínez-Vázquez, M.V. Cabañas, J.L. Paris, D. Lozano, M. Vallet-Regí *

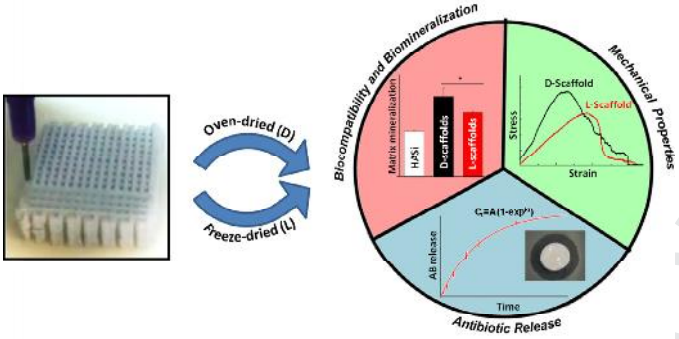

Acta Biomaterialia xxx (2015) xxx–xxx

Contents lists available at ScienceDirect

Acta Biomaterialia

journal homepage: www.elsevier.com/locate/actabiomat

Fabrication of novel Si-doped hydroxyapatite/gelatine scaffolds by rapid prototyping for drug delivery and bone regeneration

F.J. Martínez-Vázquez [a,b], M.V. Cabañas [a], J.L. Paris [a,b], D. Lozano [a], M. Vallet-Regí [a,b,*]

[a] Departamento de Química Inorgánica y Bioinorgánica, Facultad de Farmacia, UCM, Instituto de Investigación Sanitaria Hospital 12 de Octubre i+12, 28040 Madrid, Spain
[b] Networking Research Center on Bioengineering, Biomaterials and Nanomedicine (CIBER-BBN), Madrid, Spain

ARTICLE INFO

Article history:
Received 8 September 2014
Received in revised form 17 December 2014
Accepted 23 December 2014
Available online xxxx

Keywords:
Three-dimensional printing
Hierarchical porosity
Composite scaffolds
Vancomycin
Tissue engineering

ABSTRACT

Porous 3-D scaffolds consisting of gelatine and Si-doped hydroxyapatite were fabricated at room temperature by rapid prototyping. Microscopic characterization revealed a highly homogeneous structure, showing the pre-designed porosity (macroporosity) and a lesser in-rod porosity (microporosity). The mechanical properties of such scaffolds are close to those of trabecular bone of the same density. The biological behavior of these hybrid scaffolds is greater than that of pure ceramic scaffolds without gelatine, increasing pre-osteoblastic MC3T3-E1 cell differentiation (matrix mineralization and gene expression). Since the fabrication process of these structures was carried out at mild conditions, an antibiotic (vancomycin) was incorporated in the slurry before the extrusion of the structures. The release profile of this antibiotic was measured in phosphate-buffered saline solution by high-performance liquid chromatography and was adjusted to a first-order release kinetics. Vancomycin released from the material was also shown to inhibit bacterial growth in vitro. The implications of these results for bone tissue engineering applications are discussed.

1. Introduction

Synthetic biodegradable scaffolds are becoming highly promising materials for bone substitution and regeneration [1]. They can provide an adequate structural support and a 3-D system on which cells can grow and migrate while the tissue regenerates, acting as a temporary extracellular matrix inducing the natural process of tissue regeneration and development. Thus, ideal scaffolds must combine osteoinductive materials with biodegradable polymers to create a material with proper biocompatibility, bioactivity, biodegradability and toughness. This type of material should be formed, mimicking the natural tissue, by an organic phase (as collagen in bone) and an inorganic osteophilic component (similar to apatite). In addition, it is essential that these materials exhibit an interconnected architecture of pores [2] in order to facilitate bone growth, angiogenesis and transport of nutrients into them.

Among the limitations of the techniques conventionally used to fabricate scaffolds (solvent casting, fiber meshing, gas foaming, etc.) the most relevant is related to the limited control over pore structure (essentially size, distribution, and shape). These hurdles are overcome by solid freeform fabrication techniques [3–5] such as 3-D printing, robocasting and fused deposition modeling, since they use a computer-aid design (CAD) model to create complex and tailored 3-D structures layer-wise, producing optimal pore architectures to obtain desirable mechanical and diffusion properties for specific applications.

However, the use of these techniques comprises the optimization of the rheological properties of the slurries, which is a great challenge in the case of those materials constituted by different components (composites). The type and amount of additives (binders, dispersants, flocculants, etc.) and the solid loading in the slurry (preferably high to increase the strength of the scaffold) makes it difficult to fabricate such structures. Hence, the study of the optimal conditions to obtain appropriate slurries is a key step to fabricate such scaffolds.

On the other hand, the use of composite scaffolds constituted by inorganic compounds such as calcium phosphates and silicate bioactive glasses with biodegradable polymers can improve the mechanical/physical properties [6] and the degradability of the inorganic material, and moreover drug release profiles can be controlled to a greater extent than on pure ceramics [7].

In addition, drug loading into these structures improves further their functionality to treat, for example, osteomyelitis [8], and hence there is increasing interest in incorporating a drug delivery function. The implantation will be successful only if tissue

* Corresponding author at: Departamento de Química Inorgánica y Bioinorgánica, Facultad de Farmacia, UCM, Instituto de Investigación Sanitaria Hospital 12 de Octubre i+12, 28040 Madrid, Spain. Tel.: +34 913941843; fax: +34 913941786.
E-mail address: vallet@ucm.es (M. Vallet-Regí).

http://dx.doi.org/10.1016/j.actbio.2014.12.021
1742-7061/

integration occurs without significant bacterial adhesion, thus preventing colonization of the implant.

Besides, since the activity of the drugs must be preserved, the fabrication process must not degrade it. Thus, a common procedure to incorporate drugs in the scaffold is impregnation [9], which consists of immersing the scaffold in a drug solution. However, the loading output of the process is very low since a highly concentrated solution must be prepared in order to incorporate a small amount of drug in the scaffold, and hence the process is neither very well controlled and nor very cost-effective.

In this work, we have optimized the processing conditions to fabricate rapidly prototyped composite scaffolds with a high content of ceramic, and without the addition of any sort of additive (dispersant, binder, etc.) by means of a simple, fast and low-cost procedure. In order to obtain ideal synthetic scaffolds, gelatine and silicon-doped hydroxyapatite (HASi) were chosen to fabricate the composite material. Gelatine is a biocompatible product produced by the degradation of collagen, the majority phase in bone, and HASi is among the most interesting bioceramics from the bioactivity point of view. In vitro experiments, in powdered form as well as coatings, have evidenced an important improvement in the bioactive behavior with respect to nonsubstituted apatites [10–12]. This means that HASi will bind faster to the bone after implantation, ensuring osteointegration. Furthermore, an in vivo study, comparing the rates of bone apposition to HA and HASi ceramic implants demonstrated bone apposition to be significantly greater at the surface of HASi implants [13,14]. Thus, HASi/gelatine porous scaffolds were fabricated at moderate temperature by using a bioplotter system. The composition, microstructure, and mechanical and biological behaviors of these materials were evaluated. In addition, since the fabrication process of the scaffolds built in this study allows an appropriate incorporation of drugs in the slurries, the release profile of vancomycin from different scaffolds was analyzed.

To our knowledge this is the first study that reports the fabrication, under mild conditions, of rapidly prototyped drug-loaded composite scaffolds with high ceramic/organic ratios. Other authors have reported systems that rely on the setting reaction of cements, an exothermic reaction that implies acidic media, both conditions that may degrade the drug [15,16].

2. Experimental

2.1. Synthesis and preparation of HASi powder

HASi was prepared by the aqueous precipitation reaction of $Ca(NO_3)_2{\cdot}4H_2O$, $(NH_4)_2HPO_4$ and $Si(CH_3\text{-}CH_2O)_4$ (TEOS) according to the method reported elsewhere [17]. Briefly, a 1 M solution of $Ca(NO_3)_2{\cdot}4H_2O$ was added to a stoichiometric concentration of $(NH_4)_2HPO_4$ and TEOS solution in order to obtain a composition of $Ca_{10}(PO_4)_{5.75}(SiO_4)_{0.25}(OH)_{1.75}$. The reaction mix was stirred at 80 °C for 12 h, keeping the pH at 9.5 by the addition of NH_3. The white solid precipitated was filtered and washed with hot water until a neutral pH was achieved, and then dried overnight. Afterwards, the powder was calcined at 700 °C for 2 h (10 °C min^{-1} heating rate) and then milled for 1 h at 400 rpm in a planetary ball milling machine (Pulverisette 6, Fritsch), resulting in a narrow particle size distribution between 1 and 3 μm (measured by sedimentation in a Micromeritics Sedigraph 5100 Size Analyzer).

2.2. Preparation of the slurry and scaffolds

The as-prepared HASi powder and type-A gelatine (porcine skin, Sigma Aldrich) were used to make water-based slurries for rapid prototyping with a weight ratio HASi/Gelatine of 9. First, a hydrogel of gelatine was formed by mixing 1 g of gelatine and 10 g of distilled water at 45 °C. Then, the as-prepared, milled and sieved HASi powder was gradually added to the mixture. After each addition, the mixture was placed in a planetary centrifugal mixer (ARE-250, Thinky Corp., Tokyo, Japan) for a few minutes to improve its homogeneity and stability.

A similar procedure was carried out to prepare vancomycin-loaded composite scaffolds (2.0 wt.% content of vancomycin referred to the final dried solid). In this case, the hydrogel was formed by mixing 1 g of gelatine and 8 g of water. Then, 2 ml of an aqueous solution of vancomycin (100 mg ml^{-1}) was added progressively to the hydrogel simultaneously to the addition of HASi powder (9 g).

3-D scaffolds consisting of a mesh of HASi/Gelatine rods were constructed layer-wise via direct-write assembly of the composite slurry (ink) using a robotic deposition device (EnvisionTEC GmbH 3-D BioplotterTM). The printing syringe was partially filled with the ink and placed on the three-axis motion stage controlled independently by a computer-aided direct-write program (PRIMCAM version 2.98). The ink was kept at 30 °C for 10 min prior to its extrusion through deposition nozzles (Nordson EFD) with a tip diameter d = 500 μm. The gelatine concentration and temperature of extrusion were set by trial and error. Each layer in the computer 3-D model of the structure consisted of parallel rods with a spacing from center to center s = 1.4 mm. Rods in adjacent layers are perpendicularly oriented and the spacing between layers was set to h = 320 μm. The external dimensions of the scaffolds were set at about 20 mm × 20 mm × 5 mm so that in total of 15 layers were deposited.

The structures were subsequently soaked in a solution of glutaraldehyde (GA) (0.25 w/v) at 25 °C for 10 min and then washed repeatedly with distilled water to eliminate the remaining GA. Time and concentration of crosslinking were selected to minimize the effect of the toxicity of GA and preserve the structural integrity of the scaffolds [18]. In order to study the influence of the drying procedure, the structures were then divided in two groups for further treatment: (a) drying at 37 °C overnight (hereinafter D-scaffolds), or (b) lyophilizing by freezing at −80 °C and keeping a sublimation pressure of 0.05 mbar (hereinafter L-scaffolds).

2.3. Chemical and structural characterization

Elemental chemical analysis of the as-prepared HASi powder was carried out by X-ray fluorescence (XRF) spectrometry for Si, Ca and P on a Bruker-AXS S4 Explorer instrument, using Rh K_α (λ = 0.6139 A) radiation. The structure and composition of both HASi powder and HASi/gelatine scaffolds were determined by X-ray diffraction (XRD), using a Phillips PW-1800 diffractometer and Cu K_α radiation, and Fourier transform infrared spectroscopy (FTIR) in a Nicolet Nexus spectrometer.

Scanning electron microscopy (SEM), performed on a JEOL 6400 microscope/Oxford Pentafet super ATW system, was used at to analyze the micro- and macrostructure of both D- and L-scaffolds. The samples were previously gold plated. The pore size of the structures was determined by Hg intrusion porosimetry measured using a Micromeritics Autopore III 9410 porosimeter.

Density of D- and L-scaffolds (ρ_{scff}) was measured as total weight divided by external volume. Total open porosity (P) was determined from these measurements by considering the following equation:

$$P = [1 - \rho_{scff}/\rho_{He})] \times 100 \quad (1)$$

where ρ_{He} is the density of the composite measured by He pycnometry (AccuPyc 1330 Micromeritics), by using the following analysis parameters: camera volume, 3.5 cm^3; number of purges, 10;

Please cite this article in press as: Martínez-Vázquez FJ et al. Fabrication of novel Si-doped hydroxyapatite/gelatine scaffolds by rapid prototyping for drug delivery and bone regeneration. Acta Biomater (2015), http://dx.doi.org/10.1016/j.actbio.2014.12.021

purge/run fill pressure, 19,500 psig; equilibrium rate, 0.005 psig min^{-1}; number of runs, 10.

2.4. Swelling behavior

The weight and volume of D- and L-structures were measured before and after soaking in phosphate-buffered saline solution (PBS) several times in order to evaluate the swelling behavior of the scaffolds in this medium. The gravimetric and volumetric swelling degree (S_W and S_V, respectively) of the structures was determined according to the following equation:

$$\text{Swelling} = 100 \times (M_t - M_b)/M_b \quad (2)$$

where M_b corresponds to the weight/volume of the structure before soaking in PBS and M_t to the weight/volume of the structure after soaking for a specific time. Weighted dry scaffolds of around (8–9) mm × (7–8) mm × (4–5) mm were used for this study. To calculate the S_w, the weight is measured after the scaffold is dried with filter paper. The scaffolds dimensions are measured with a micrometer. The measurements were repeated in three locations along the specimen. The data were averaged over three samples.

2.5. Contact angle measurements

Static contact angle measurements were carried out on dry bulk samples using a contact angle measuring instrument (CAM200, KSV Instruments, Finland). Disks of HASi and HASi/gelatine were made by milling the as-prepared powder and the composite scaffold respectively, and shaping them by uniaxial compression in a cylindrical die with a diameter of 15 mm. Gelatine films were also prepared by casting the above-mentioned gelatine hydrogel into glass Petri dishes and then soaking them in a GA solution (0.25 w/v) for 10 min. Finally, the gelatine disks were dried at 37 °C overnight. Distilled water (3 µl) was added to the different disks by a motor-driven syringe at room temperature. Reported data were obtained by averaging the results of five measurements.

2.6. Mechanical characterization

The compressive strength of the dry structures (D- and L-scaffolds) was determined by performing uniaxial tests on approximately cubic blocks of 4 mm per side cut from the 3-D-printed specimens after the crosslinking. The tests were carried out in air on a universal testing machine (AG-IS10kN, Shimadzu Corp., Kyoto, Japan) at a constant crosshead speed of 0.6 mm min^{-1}. Tests were performed in the direction perpendicular to the printing plane. The load vs. displacement curve was recorded during the tests. The compressive strength of the structure was calculated as the maximum applied load divided by the measured square section of the sample. A minimum of 20 samples were tested in each testing condition in order to obtain statistically reliable values. Toughness was estimated as the strain energy density (G), as reported by other authors [19], from the integral of the nominal stress–strain curve at the strain value corresponding to the compressive strength (G_{max}).

2.7. Biological characterization

Cell culture experiments were performed using the well-characterized mouse osteoblastic MC3T3-E1 cell line (subclone 4, CRL-2593; ATCC, Manassas, VA), widely used in biomaterial in vitro validations [20–22]. The D- and L-scaffolds were placed into each well of 6- or 24-well plates before cell seeding for the whole experimental period. Ceramic scaffolds without gelatin, HASi [23], were also studied for comparison. The thickness of the scaffolds used in these in vitro studies was 4–5 mm, and the dimensions of the samples used were 5 mm × 5 mm for 24-well plates and 10 mm × 10 mm for 6-well plates. Then, MC3T3-E1 cells were plated at a density of 10.000 cells cm^{-2} in 2 ml of osteogenic medium consisting of α-minimum essential medium containing 10% heat-inactivated fetal bovine serum (FBS), 50 µg ml^{-1} ascorbic acid, 10 mM β-glycerol-2-phosphate and 1% penicillin–streptomycin at 37 °C in a humidified atmosphere of 5% CO_2, and incubated for different times. Some wells contained no scaffolds as controls. Medium was replaced every other day. The measurement of cell proliferation, alkaline phosphatase (ALP) activity and gene expression was performed both in cells present on the well after withdrawing the scaffolds and in cells present inside the scaffolds. Both types of experiments provided very similar results and only the results of the cells present on the culture wells are shown for clarity.

Cell proliferation was assessed after MC3T3-E1 cell incubation in 24-well plates with the different materials for 2 and 5 days. At this time, Alamar Blue solution (AbD Serotec, Oxford, UK) at 10% (v/v) was added to the cell culture. Four hours thereafter, 1 ml samples of the cell-conditioned medium were added to a 24-well plate and fluorescence intensity was measured using excitation and emission wavelengths of 540 and 620 nm, respectively. Following incubations with the tested materials for 5 days, these cells were washed with PBS, and ALP activity was measured in cell extracts obtained with 0.1% Triton X-100 using *p*-nitrophenylphosphate as substrate, as described previously [20,22]. ALP activity was normalized to cell protein content, determined by the bicinchoninic acid (BCA) method (Thermo Scientific, Rockford, IL, USA) with bovine serum albumin as standard. Matrix mineralization in MC3T3-E1 cells exposed to the tested materials for 10 days was determined using Alizarin Red S staining, measuring absorbance at 620 nm as described [20,21].

Total RNA was isolated from cells cultured on 6-well plates by a standard procedure (Trizol, Invitrogen, Groningen, the Netherlands), and gene expression of various osteoblastic products was analyzed by real-time polymerase chain reaction (PCR) using an ABI PRISM 7500 system (Applied Biosystems, Foster City, CA), as reported [20,22]. Unlabeled mouse specific primers for Runx2, osteocalcin (OC), vascular endothelial growth factor (VEGF) and TaqManMGB probes were obtained by Assay-by-DesignSM (Applied Biosystems). The mRNA copy numbers were calculated for each sample by using the cycle threshold (Ct) value. 18S rRNA, a housekeeping gene, was amplified in parallel with the tested genes. Fold change for the treatment was defined as the relative expression compared with that of the control and was calculated as $2^{-\Delta\Delta C}$, where ΔΔCt = ΔCtreatment − ΔCcontrol.

On the other hand, a cytotoxicity MTT test was performed in order to analyze cytotoxicity induced by the materials. MC3T3-E1 cells were plated at a density of 10.000 cells cm^{-2} in 12-well plates containing 1.5 ml of α-minimum essential medium containing 10% heat-inactivated fetal bovine serum (FBS) and 1% penicillin–streptomycin at 37 °C in a humidified atmosphere of 5% CO_2. At 24 h, the scaffolds (5 mm × 5 mm × 5 mm) were placed into a cell culture insert (Transwell® 12 mm inserts, 0.4 µm pore size polycarbonate membrane, Corning Inc., NY, USA) filled with 300 µl of this medium and incubated for 24 h. Then, the cells were incubated with Thiazolyl Blue Tetrazolium Bromide for 4 h. A positive control was performed with 300 µl of GA solution in the cell culture insert (same concentration as used for scaffold crosslinking), in order to verify the GA diffusion through the insert membrane. The absorbance at 570 nm (due to formazan, dissolved in dimethylsulfoxide) was then measured using an Unicam UV-500 UV–visible spectrophotometer.

Please cite this article in press as: Martínez-Vázquez FJ et al. Fabrication of novel Si-doped hydroxyapatite/gelatine scaffolds by rapid prototyping for drug delivery and bone regeneration. Acta Biomater (2015), http://dx.doi.org/10.1016/j.actbio.2014.12.021

2.8. In vitro drug release and bacterial growth inhibition

Vancomycin release experiments were carried out by submerging L- and D-scaffolds (10 mm × 10 mm × 5 mm) in 20 ml of sterile PBS at 37 °C and pH 7.4 under mechanical oscillation. Aliquots of 100 µl were taken at 10, 20, 30, 60, 120, 180, 360, 480 min and 24 h and then stored at 5 °C. Three samples of each type of material were used.

Vancomycin concentration released from loaded scaffolds was monitored by reverse-phase high-performance liquid chromatography (HPLC) in an Agilent automatic analysis system composed of a Model #2695 separations module coupled to a Model #2696 photodiode array detector and controlled by Empower2 software (Waters, Milford, MA). Chromatographic separations were carried out with a 150 mm × 4.6 mm pre-packed analytical MediterraneaTM Sea18 column (Teknokroma, Sant Cugat del Vallès, Spain) containing 5 µm C18 functionalized silica beads. The isocratic mobile phase consisted of a mixture of 20 mM NaH_2PO_4–Na_2HPO_4 buffered solution at pH 6.9 and acetonitrile (88:12, v/v) and was delivered at 1.0 ml min^{-1} at 37 °C. The injection volume was 10 ml and detection was performed with UV light at a wavelength λ = 280 nm. Under these conditions, the retention time was 4.1 min. Vancomycin solutions at concentrations of 0, 0.0675, 0.125, 0.25, 0.5 and 1 mg ml^{-1} were used as standards.

Agar disk diffusion tests (ADTs) were used to examine the antibacterial effect of vancomycin-loaded materials [24]. To carry out ADTs, we prepared slurries with and without drug (as previously described), and disks (11 mm diameter, 4 mm height) were obtained. Afterwards, they were crosslinked for 10 min and dried according the two previously described procedures. The surface of solid agar in Petri dishes was inoculated with a suspension of *Staphylococcus aureus* bacterial culture with a cell concentration of 1.3 × 10^{10} bacteria ml^{-1}. Then, the disks were placed on the bacteria-inoculated agar plates followed by incubation at 37 °C for 24 h. After that, the bacterial inhibition zone size was measured.

3. Results and discussion

Fig. 1 shows an example of a scaffold while printing and an as-extruded scaffold after crosslinking and prior to the drying treatment. The scaffold exhibits the advantage of easy shaping by cutting since the wetted state provides a soft material that maintains enough structural integrity to be manipulated, and hence is of interest for surgical requirements such as the adjustment of the external geometry of the implant to the bone defect.

3.1. Chemical characterization of HASi powder and HASi/gelatine scaffolds

XRF analysis of as-prepared HASi powder shows that the experimental composition is very similar to the nominal composition with a Si content of ~0.7 wt.% (0.25 mol) and a Ca/(P + Si) ratio of 1.67. The XRD pattern of the synthesized powder (Fig. 2a) indicates that all the diffraction maxima correspond to the reflections of an apatite phase (JCPDS 2003 powder diffraction file 9-432) and traces of other calcium phosphate impurities were not detected by this technique. The average crystal size, determined from the width of different XRD maxima by applying the classical Scherrer formula, was 35 ± 5 nm, indicating that this type of powder is nanocrystalline in scale, which is desirable to improve cell adhesion and proliferation [25].

The FTIR spectrum of the HASi powder (Fig. 2b) shows vibration bands characteristic of hydroxyapatite [26]. These bands appear at 3569 and 629 cm^{-1} because of the stretching and vibrational mode of hydrogen-bonded OH groups, respectively, and the bands corresponding to $(PO_4)^{3-}$ group appear at 1087 (ν3) and 1022 (ν3), 960 (ν1), 598 (ν4) and 561 cm^{-1} (ν4). Moreover, the as-prepared HASi powder contains a small amount of $(CO_3)^{2-}$ (appearance of small vibration bands at 890, 1410 and 1457 cm^{-1}) which can be formed by the hydrolysis and decomposition of $Si(CH_3\text{-}0CH_2O)_4$ precursor, while other groups such as nitrates or ammonium, from the raw materials, cannot be detected [17].

On the other hand, the XRD pattern corresponding to the composite HASi/gelatine scaffold is very similar to that of the ceramic powder, and is not shown for the sake of clarity. The FTIR spectrum (Fig. 2b), besides presenting all the bands described above (due to HASi), shows several bands corresponding to gelatin: amide bands at ~1650 cm^{-1} (C=O stretching) and ~1550 cm^{-1}

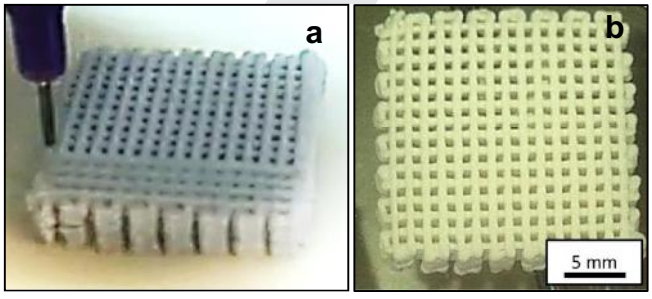

Fig. 1. Optical image captured in situ during the printing of a scaffold (a) and a photograph of a HASi/gelatine scaffold as fabricated (b).

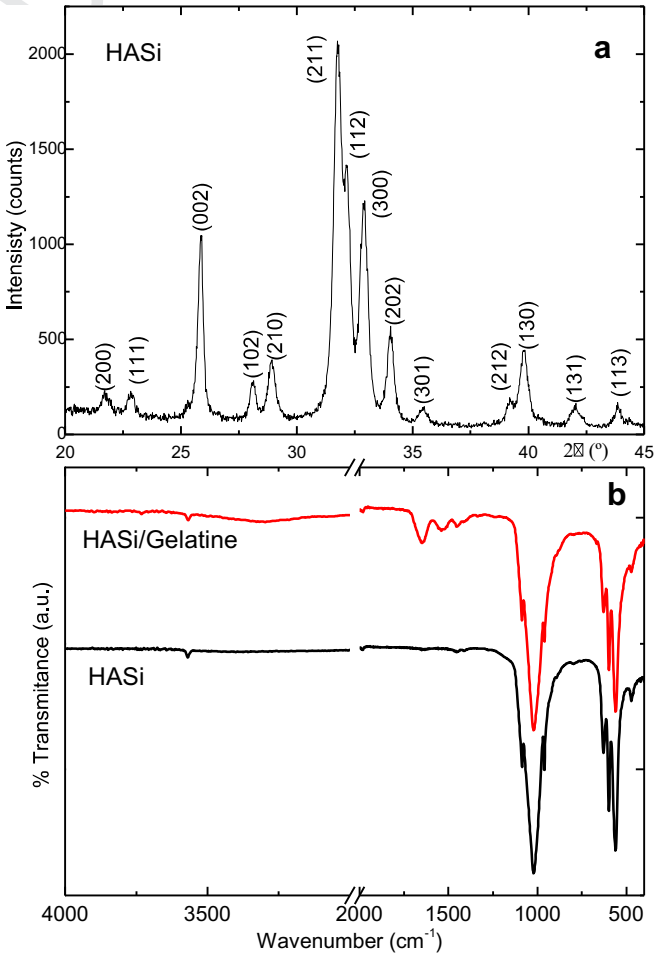

Fig. 2. XRD pattern of HASi powder (a) and FTIR spectra corresponding to HASi powder and HASi/Gelatine scaffold (b).

Please cite this article in press as: Martínez-Vázquez FJ et al. Fabrication of novel Si-doped hydroxyapatite/gelatine scaffolds by rapid prototyping for drug delivery and bone regeneration. Acta Biomater (2015), http://dx.doi.org/10.1016/j.actbio.2014.12.021

(N—H deformation), as well as other bands that appear at ~1380 and ~1440 cm^{-1} that are due to the amino acids in the gelatine structure [18]. Therefore, the process of scaffold preparation did not result in any detectable change in the chemical structure of gelatine. The peak attributed to the characteristic carbonyl bond (C=O) of the aldehyde group at ~1700 cm^{-1} does not appear in the FTIR spectra of HASi/gelatine crosslinked samples, which indicates that no excess of unreacted GA remains in the structure. Considering its cytotoxic potential [18], the elimination of GA from the scaffold is highly desirable. The absence of such chemical in the structure can be caused by the fact that the majority of the GA molecules have reacted with gelatine, and/or unreacted GA was completely washed out from crosslinked scaffolds.

3.2. Structural characterization of scaffolds

SEM micrographs of Fig. 3 show the morphology and architecture of both L- and D-scaffolds at low and high magnification. It can be seen that although no sintering procedure has been carried out on these materials to strengthen the rods, they maintain their shape after the extrusion without collapsing with the inferior layers, and the cylindrical sections of the rods essentially preserve their shape, with a minor degree of deformation. The network of interconnected macropores (Fig. 3a–d) designed by rapid prototyping are evident in the different perspectives. In this sense, the predesigned pores that are oriented parallel to the printing plane (Fig. 3a and b) exhibit apparent differences in pore size; while the rods of L-scaffolds are clearly separated, the struts of D-scaffolds are located much closer to each other, thus creating narrower cavities along this direction. The differences in the macropore size between L- and D-scaffold are even more noticeable in Fig. 3c and d. This could be attributed to the greater contraction that occurs in the latter struts during the drying treatment, which is evidenced by the variations of the rod diameter of the L- and D-structures (560 ± 60 and 477 ± 43 μm, respectively), and is extended to a reduction of macropore size (601 ± 50 μm for L-scaffolds, and 514 ± 14 μm for D-scaffolds).

In addition, small cavities are apparent at lower scale (Fig. 3e–h), probably due to the elimination of water during the post-printing treatment. Moreover, it is noticeable that the microscale morphology of both kinds of struts is uniform either within the rods and on their surface, and no sediments of gelatine or apatite are evident, which indicates that all the components are well dispersed in the slurry prior to its extrusion.

The Hg intrusion porosimetry of Fig. 4 shows a bimodal interconnected pore size distribution for both sorts of samples, with the smaller distribution centered at 33 nm for both sorts of samples and related to the in-rod porosity, and the greater one at 340 μm for D-scaffolds and 400 μm for L-scaffolds, corresponding to the predesigned porosity (both macropore sizes being suitable for osteoblast cell growth [27]). This finding is in good agreement with the SEM observations. However, although it was mentioned above that there is a perceptible porosity in the micrometric range (Fig. 3e–h), there is no actual peak in the porosimetry graph that could be associated with that pore size, which indicates that those pores are closed, and/or open but unconnected, and the interconnectivity is only effective at the two ranges determined by the bimodal distribution.

The density value measured by He pycnometry for HASi/gelatine was 2.611 ± 0.005 g cm^{-3}. This value is in good agreement with that determined by the rule of mixtures, taking into account the composition of the structures (90% HASi and 10% gelatine) and the values of density measured for gelatine and HASi powder (1.25 ± 0.01 and 2.91 ± 0.01 g cm^{-3}, respectively). On the other hand, the total open porosity of the samples was calculated (Eq. (1)) to be 84 ± 6% for L-scaffolds and 80 ± 4% for D-scaffolds.

3.3. Swelling behavior

Regarding the swelling behavior, the results show a rapid increase in water absorption in the first 15 min, and this was kept

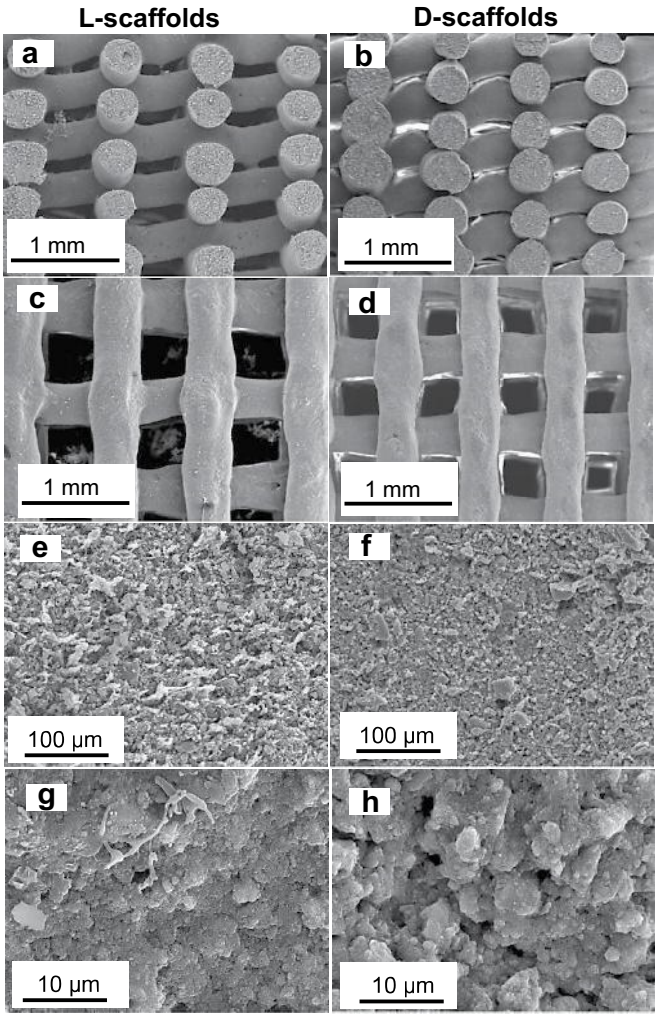

Fig. 3. SEM micrographs corresponding to L- and D-scaffolds: (a, b, e, f) lateral view; (c, d, g, h) top view.

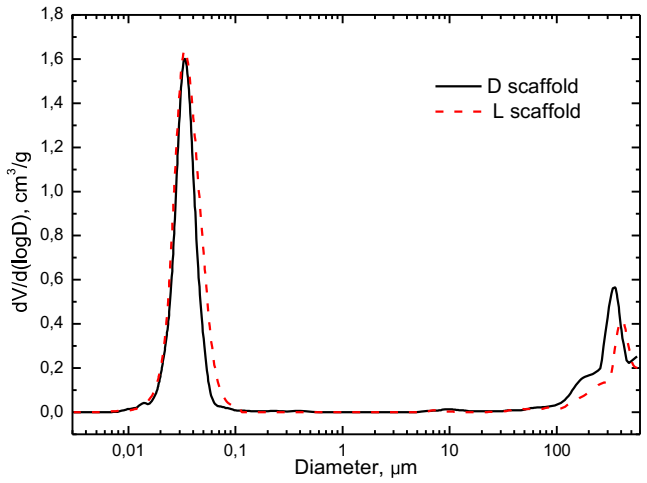

Fig. 4. Pore size distribution of the D- and L-scaffolds.

Please cite this article in press as: Martínez-Vázquez FJ et al. Fabrication of novel Si-doped hydroxyapatite/gelatine scaffolds by rapid prototyping for drug delivery and bone regeneration. Acta Biomater (2015), http://dx.doi.org/10.1016/j.actbio.2014.12.021

unaltered for further periods of time after equilibrium had been achieved. The gravimetric swelling ratio, Eq. (2), is greater in the case of L-scaffolds (S_W = 68.6 ± 1.1% vs. 57.4 ± 1.2% for D-scaffolds) since they exhibit a wider open architecture, and so more liquid is accessible to penetrate within the in-rod porosity. However, the volumetric swelling ratio is greater in the case of D-scaffolds (S_V = 9.7 ± 0.5% vs. 2.6 ± 0.2% for L-scaffolds) since the contraction produced in these structures, due to the elimination of water during the drying treatment, is counteracted when the material retains liquid. On the other hand, according to the microstructural analysis mentioned above, L-scaffolds do not exhibit shrinkage after treatment since the elimination of water in the step from solid to gas preserves the initial architecture, and so there are no such counteracting phenomena.

3.4. Surface hydrophilicity measurements

Since surface hydrophilicity has been reported to significantly affect the biological performance of materials, such as protein adsorption, cell attachment, migration and spreading [28,29], the water contact angle was measured to evaluate and compare the surface hydrophilicity of the hybrid material fabricated in this study and its components. Fig. 5 shows the contact angles formed by water drops on smooth surfaces of gelatine, HASi/gelatine composite and HASi. The contact angle corresponding to gelatine substrate indicates that this component of the hybrid scaffold contributes to minimize the hydrophilicity of the composite, since it is clearly superior (73 ± 2°) to that of the ceramic component (30 ± 1°). However, the contact angle corresponding to the composite substrate (38.6 ± 0.2°) does not greatly surpass the angle formed by the ceramic disk, which is certainly caused by the low content of gelatine in the composite (10 wt.% vs. 90 wt.% of ceramic). Nonetheless, the contact angle corresponding to the composite substrate is in a good range for wettability and this substrate should therefore offer adequate cell–material interaction according to previous studies on self-assembling monolayers of organosilanes [30], where human fibroblasts exhibited better growth due to an increase of protein adsorption on moderately wettable substrates, or plasma-treated polytetrafluoroethylene surfaces [31] that showed low detachment of endothelial cells for angles between 20 and 45°. Nonetheless, we assume that the adhesion process is not exclusively governed by the wettability of the surfaces, but also by chemical characteristics.

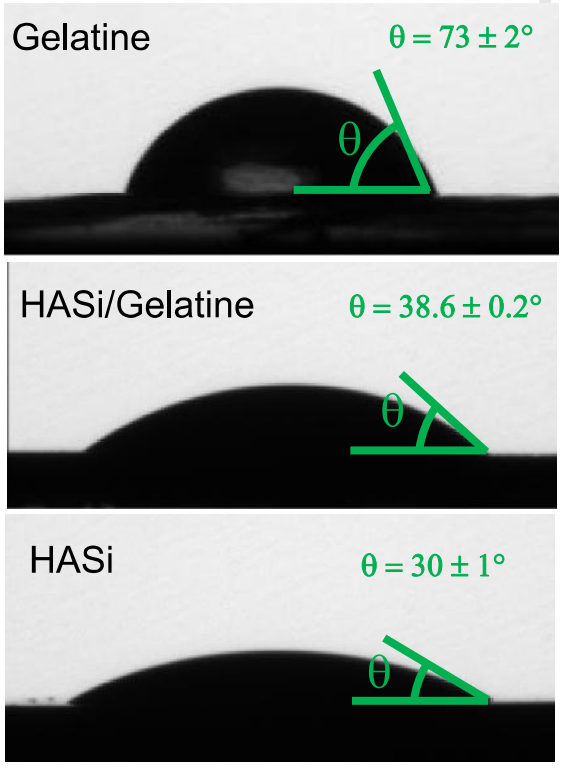

Fig. 5. Micrographs showing water drop profiles on different material surfaces. Contact angles were determined as indicated.

3.5. Mechanical characterization

Fig. 6a shows representative nominal stress–strain curves from uniaxial compressive tests performed on D- and L-scaffolds. The successive load drops observed in these plots are associated with the crack pop-in events responsible for the fracture of composites with this type of structure [32]. The onset of the first of these cracks occurs during the elastic regime (i.e. within the linear regions of the curves), and usually corresponds to the maximum applied stress, thereby determining the compressive strength of the scaffold. The stress decline after the maximum is abrupt, indicating that the structure failure is catastrophic. Although some little mechanical resistance remains after multiple cracking events, this residual load-bearing capacity is an artefact since it is provided by disconnected pillars that collapse when the load is removed.

The maximum applied stress in the L-scaffolds is reached at greater strain values (0.09) than in D-scaffolds (0.06), indicating that the elastic regime in former structures is wider. The typical spongy behavior of gelatine after the freeze-drying process could be responsible for this more noticeable elastic behavior in L-scaffolds. Moreover, the slope of the stress–strain curves corresponding to these structures is lower than that of D-scaffolds, which is indicative of a larger compliance as a result of its slightly superior porosity.

In addition, the compressive strength of D-scaffolds (3.8 ± 1.1 MPa) is greater than that of L-scaffolds (2.7 ± 0.8 MPa), which is also evidenced in Fig. 6b. This difference in the compressive strength can be also attributed to the variation of porosity exhibited by these structures. Moreover, the level of strength that is achieved by our structures is due to the effect that the crosslinking has on the gelatine distributed among apatite crystals, providing a structural integrity. On the other hand, a comparison of the compressive strength of our structures with results from the literature for pure HA scaffolds fabricated by conventional and solid free from fabrication techniques [27–51] reveals that, in spite of the fact that no thermal treatment has been carried out in our structures, their strength is superior to some analogous structures with similar or even greater density. Moreover, the compressive strength of our scaffolds is similar to that corresponding to bone tissues of the same apparent dry density (shaded region in Fig. 6b), lying slightly under the compressive strength values corresponding to such specimens. In any case, the compressive strength for structures with similar porosity could be improved by reducing the proportion of ceramic in the slurry to ~60 wt.% [52], due to a better embedding of the apatite crystals in the gelatine matrix, although lower stiffness would be expected [53], which is not desirable to ensure that the stress field is transmitted to the surrounding tissue in order to promote osteoblast activity. Nonetheless, the strength achieved by these structures can be considered sufficient for safe handling in the laboratory and manipulation during surgical intervention. Moreover, since these materials behave like a hydrogel, they provide the advantage that their shape is easily adjustable, in wet conditions, to that of the bone defect (in situ) during surgery.

The strain energy densities of our structures are similar regardless the drying treatment (0.15 ± 0.05 J cm^{-3} for L-scaffolds and

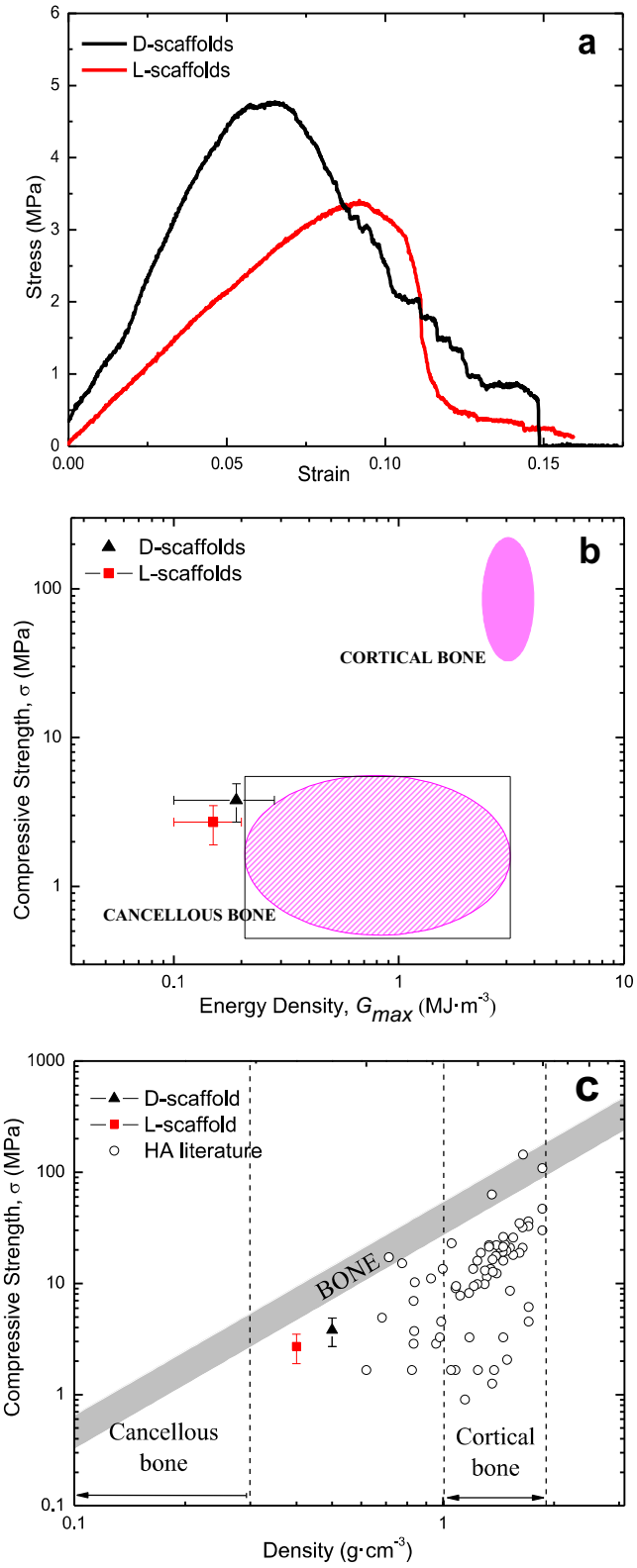

Fig. 6. Representative stress–strain curves obtained from uniaxial compressive tests performed on L- and D-scaffolds (a), plot of strength vs. strain energy density of L- and D-scaffolds compared to bone properties (b), and comparative plot of strength of data from this work and literature reports (not distinguished) (c); the results are plotted as a function of material density (bottom axis), and the shaded bands represent bone properties (including data dispersion) as a function of apparent bone dry density, according to a model given by Keller [63].

0.19 ± 0.09 J cm^{-3} for D-scaffolds), as shown in the Ashby diagram of Fig. 6c, and their values lie close to the range of trabecular bone [54]. The strain energy density achieved under compression for our structures is far superior to reported values obtained for sintered calcium phosphate scaffolds with lower porosity, and similar to the fracture energy of these materials after coating with polycaprolactone [19,55]. These results are not trivial, considering that the structures described here have not been sintered to improve their strength by intergranular fusing, and are highly porous (80–84 vol.%). Indeed, greater fracture energies could be achieved in the case of structures with higher gelatine contents [18,56], or lower porosities, by the design of smaller macropores. In any case, this considerable level of toughness could be explained in view of the magnitude of the strain reached just before fracture, especially in the case of L-structures, which is notably high (~0.09), taking into account that most of the structure is ceramic, while fracture strains do not surpass 0.07 for bone specimens [57]. This strain increase could be attributed to the flaw healing that the organic phase produces, bridging the crack walls and holding the structure together after the ceramic skeleton fails.

3.6. Biological characterization

When testing the scaffolds in osteoblastic MC3T3-E1 cells, it was observed that none of the studied materials (D-,L-scaffolds and HASi scaffolds) induced significant cytotoxicity measured by the standard MTT assay (cell viability was in all cases >98.15% that of the control). The presence of L-scaffolds failed to affect cell proliferation (2 and 5 days) but this was significantly increased with the D-scaffolds (Fig. 7a). In this regard, a significant particle release from the L-scaffolds was detected by flow cytometry (data not shown) [58]. This might explain why these types of materials did not increase cell proliferation compared to HASi scaffolds. In addition, both materials (D- and L-scaffolds) significantly increased ALP activity and matrix mineralization in MC3T3-E1 cells, compared to the HASi, at 5 and 10 days of culture, respectively (Fig. 7b). We analyzed the gene expression of two osteogenic markers (Runx2 and OC), corresponding to early and late osteoblast differentiation, respectively, and that of a key angiogenic factor, VEGF, in these cells exposed to the different scaffolds. We found that D- and L-scaffolds significantly increased the gene expression of all of these markers tested at day 5 (Fig. 7c). These positive results obtained with D- and L-scaffolds were similar to or better than those observed in related systems prepared by other methods [18,20]. Therefore, the presence of gelatine in the scaffolds improves the interaction of osteoblastic cells with these materials (and around the scaffolds), showing good cell response in terms of proliferation and differentiation (matrix mineralization and osteoblastic gene expression). These results might indicate the potential impact on the bone milieu in vivo, although the limitations of in vitro studies with transformed cells should also be taken into account.

3.7. Vancomycin-loaded scaffolds, release study and "in vitro" bactericidal efficacy

The fabrication process described here offers the feasibility of fabricating slurries for 3-D printing that can incorporate therapeutic substances in their composition. Taking advantage of this possibility, we incorporated vancomycin (a glycopeptide isolated from *Streptomyces orientalis* which is used to treat infections caused by Gram-positive bacteria [59] including methicillin-resistant staphylococcus) into our scaffolds. Thus, D- and L-scaffolds

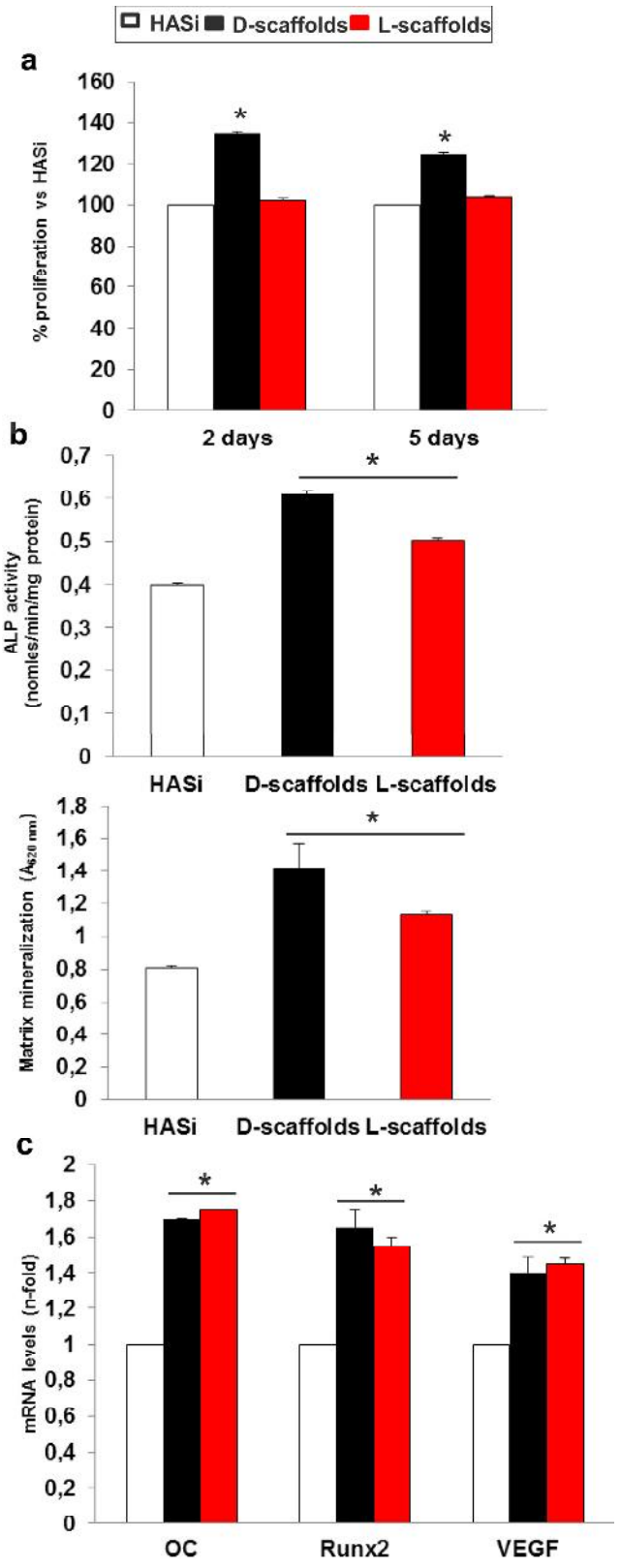

Fig. 7. MCT3T3-E1 cell proliferation (measured by Alamar Blue assay) at day 2 and 5 of culture (a), ALP activity and matrix mineralization at 5 and 10 days of cell culture (b) and gene expression (by real-time PCR) of Runx2 and OC (osteogenic markers) and VEGF (angiogenic factor) at day 5 of cell culture (c). All measurements were carried out in the presence of D- and L-scaffolds and compared to HASi scaffolds. (Data of cells without scaffolds are similar to cells with HASi scaffolds and they are not shown for clarity.) Results are mean ± standard error of the mean ($n = 4$). *$P < 0.01$ vs. HASi scaffolds.

loaded with this antibiotic (2 wt.%) and crosslinked for 10 and 20 min were fabricated. The rheological properties of the slurries were not significantly modified by the addition of vancomycin, and the same conditions for non-loaded scaffolds were used. The presence of vancomycin in the scaffolds was confirmed by FTIR analysis, showing absorption bands at 3450, 1655, 1504 and 1231 cm^{-1} (data not shown) for hydroxyl stretching, C=O stretching, C=C stretching and phenols [60].

Fig. 8a shows that the systems crosslinked for 20 min reach a lower maximum concentration of antibiotic released from the scaffolds than those structures crosslinked for 10 min, which is due to the transference of vancomycin from the struts to the crosslinking solution prior to the release study carried out in PBS. Thus, whilst the initial concentration of vancomycin loaded in the slurries was 2 wt.%, the maximum concentration for vancomycin for the scaffolds crosslinked for 20 min was 1.2 ± 0.1 wt.%; instead, the maximum concentration for D- and L-scaffolds crosslinked at 10 min was 1.6 ± 0.1 wt.%. Some removal of vancomycin from the scaffolds is also due to the washing process carried out to eliminate the unreacted GA. Vancomycin was undetectable by FTIR analysis (data not shown) on the scaffolds after the period of maximum release, which indicates that essentially all the antibiotic was delivered. In addition, the analysis of the UV spectra for all the systems revealed that no degradation of the antibiotic occurred either during the fabrication process or during drug release for the times studied here.

The release profile followed by such systems are similar (Fig. 8b), and can be described by the Noyes–Whitney equation [61]:

$$C_t = A(1 - \exp^{kt}) \quad (3)$$

where C_t is the cumulative concentration of antibiotic released at a certain time (t), A is the maximum concentration of antibiotic released and k is the release constant.

The normalized vancomycin release of the four systems (Fig. 8b) follows an almost identical first-order release kinetics, as indicated by the correlation coefficients to the above-mentioned equation. However, it is not possible to elucidate which mechanism is responsible for such release profile. Moreover, the initial burst release is notably low if not nonexistent, considering that <30% of vancomycin is released from the scaffolds at 1 h, which is actually a very sustained release taking into account that the total amount of antibiotic is delivered at 8 h. Indeed, since the scaffolds contain a hydrogel that undergoes a certain degree of swelling that reaches its maximum during the first 15 min of soaking, a relatively high drug release could be expected at that time; however, HPLC measurements reveal that <9 wt.% of the vancomycin in the scaffold is released to the PBS solution at that time. This phenomenon is attributed to the greater influence that the ceramic component of the scaffold has over the hydrogel in the antibiotic release process, which is logical considering that the apatite phase is present in a greater proportion in the material compared to the hydrogel (9:1). Moreover, since the interconnectivity into the struts of the scaffolds is limited to a low size scale range (35 nm), the entrapment of vancomycin is sufficient to maintain a gradual release through this connection, thus preventing a rapid transference of antibiotic to the PBS solution.

This explanation for the release profile of our systems is also in agreement with the fact that crosslinking time does have any influence on the antibiotic release profile of the scaffolds. In this sense, if drug release was controlled by gelatine, the crosslinking degree of this component would alter the kinetics of the systems, except in the case that gelatine was fully crosslinked at 10 min. However, it was not possible to elucidate that a partial crosslinking is achieved at shorter times, since scaffolds crosslinked for 5 min lost

Please cite this article in press as: Martínez-Vázquez FJ et al. Fabrication of novel Si-doped hydroxyapatite/gelatine scaffolds by rapid prototyping for drug delivery and bone regeneration. Acta Biomater (2015), http://dx.doi.org/10.1016/j.actbio.2014.12.021

their structural integrity, thus precluding the possibility of determining the antibiotic release accurately.

The comparison of the vancomycin release systems described in this study with other porous scaffolds [62] reveals that, although longer release periods can be achieved, the burst effect is considerably more remarkable than that reported in our study. These systems become a better choice than a systemic administration of the antibiotic, since they provide an incorporation of the drug in the implant surroundings, which is crucial prior to the vascularization of bone. Furthermore, the localized release of therapeutic substances can reduce the dose required to achieve a biological response compared to systemic delivery.

As can be seen in Fig. 8c, vancomycin-loaded disks (D-, L-Disk-V) inhibit bacterial growth (outer diameter of the inhibition zone ~18 mm), while disks without drug (D-, L-Disk) fail to inhibit bacterial growth. These results indicate that drug-loaded materials can provide an effective antibiotic concentration (above the minimum inhibitory concentration) under these in vitro conditions. These results are further proof that the drug is not degraded during the fabrication process, and it retains its bactericidal efficacy.

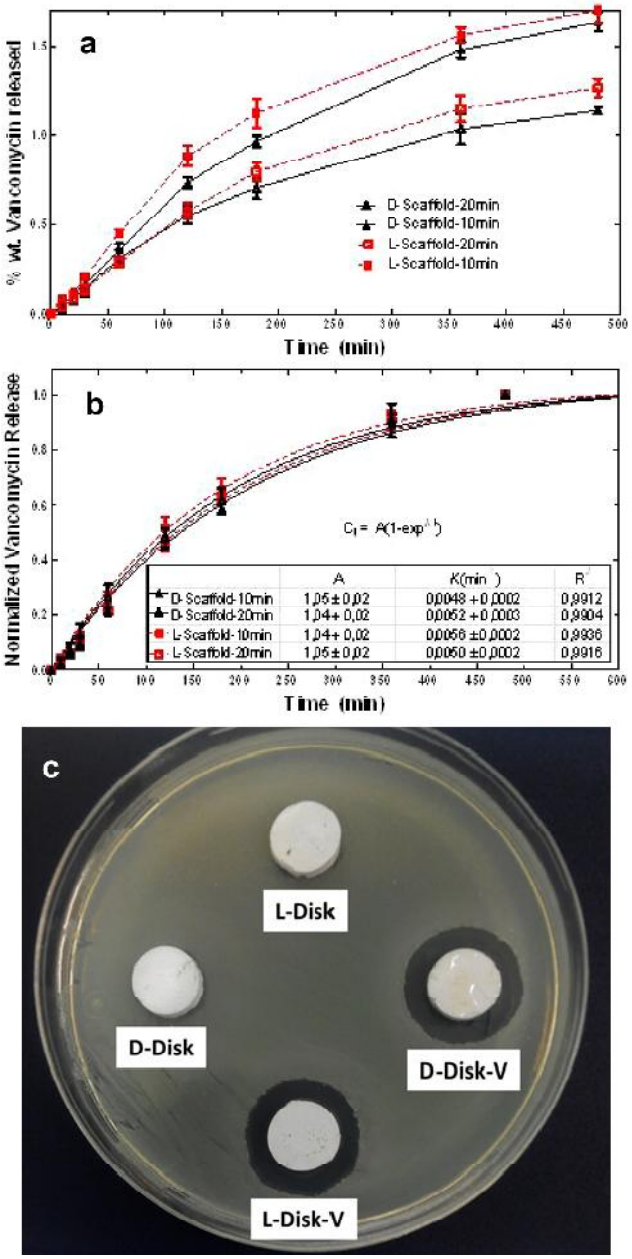

Fig. 8. (a) Vancomycin release from the scaffolds, crosslinked at 10 and 20 min, vs. time. (b) Fitting of the release profiles to the Noyes–Whitney equation and kinetic parameters of vancomycin release from the different scaffolds. (c) Agar disk-diffusion test showing bacterial growth inhibition.

4. Conclusions

A composite porous 3-D scaffold for bone regeneration and drug release capability has been fabricated by rapid prototyping in a single step at room temperature. The scaffold behaves as a hydrogel, easing the fitting to the bone defect during surgery. These scaffolds show an adequate macropore architecture for vascularization and a microporosity that enables fluid exchange, which is important for bone healing. The compressive behavior of such scaffolds is similar to that of trabecular bone of the same density, thus allowing these materials to be used under mechanical forces in a range that can be reached during surgery. In vitro cellular studies obtained with the well-established osteoblastic cell line MC3T3-E1 reveal several benefits of gelatine inclusion in the material in terms of cell differentiation and gene expression. The incorporation of the antibiotic under mild conditions during the fabrication process did not lead to drug degradation. Vancomycin is released to the medium gradually in the short term, effectively inhibiting bacterial growth around the material. This should provide a therapeutic concentration of the drug at the site of implantation when the scaffold is not yet vascularized and, therefore, systemic administration may not provide a successful clinical outcome. The findings shown in this work indicate that these composite scaffolds can be used as matrices for bone regeneration and drug delivery.

Acknowledgements

Financial support from Ministerio de Economía y Competitividad, Spain (Project MAT2012-35556 and Project CSO2010-11384-E, Ageing Network of Excellence) is gratefully acknowledged. The XRD/XRF and SEM measurements were performed at CAI Difracción de Rayos X and Microscopia Electrónica, UCM, respectively. The authors of this work would like to thank the collaboration of Dr. Pedro Miranda and Prof. Antonia Pajares, from the University of Extremadura, for the mechanical characterization.

Appendix A. Figures with essential color discrimination

Certain figures in this article, particularly Figs. 1, 2, and 4–8 are difficult to interpret in black and white. The full color images can be found in the on-line version, at http://dx.doi.org/10.1016/j.actbio.2014.12.021.

References

[1] Arcos D, Boccaccini AR, Bohner M, Díez-Pérez A, Epple M, Gómez-Barrena E, et al. The relevance of biomaterials to the prevention and treatment of osteoporosis. Acta Biomater 2014;10:1793–805.
[2] Flautre B, Descamps M, Delecourt C, Blary MC, Hardouin P. Porous HA ceramic for bone replacement: role of the pores and interconnections – experimental study in the rabbit. J Mater Sci – Mater Med 2001;12:679–82.
[3] Sachlos E, Czernuszka JT. Making tissue engineering scaffolds work. Review: the application of solid freeform fabrication technology to the production of tissue engineering scaffolds. Eur Cell Mater 2003;5:29–39 [discussion 39–40].
[4] Hollister SJ. Porous scaffold design for tissue engineering. Nat Mater 2005;4:518–24.
[5] Giannitelli SM, Accoto D, Trombetta M, Rainer A. Current trends in the design of scaffolds for computer-aided tissue engineering. Acta Biomater 2014;10:580–94.
[6] Rezwan K, Chen QZ, Blaker JJ, Boccaccini AR. Biodegradable and bioactive porous polymer/inorganic composite scaffolds for bone tissue engineering. Biomaterials 2006;27:3413–31.

[7] Habraken WJEM, Wolke JGC, Mikos AG, Jansen JA. Injectable PLGA microsphere/calcium phosphate cements: physical properties and degradation characteristics. J Biomater Sci Polym Ed 2006;17:1057–74.
[8] Brady RA, Leid JG, Costerton JW, Shirtliff ME, Angeles L. Clinical microbiology newsletter osteomyelitis: clinical overview and mechanisms of infection 2006;28:65–72.
[9] Mouriño V, Boccaccini AR. Bone tissue engineering therapeutics: controlled drug delivery in three-dimensional scaffolds. J R Soc Interface 2010;7:209–27.
[10] Hijón N, Cabañas MV, Peña J, Vallet-Regí M. Dip coated silicon-substituted hydroxyapatite films. Acta Biomater 2006;2:567–74.
[11] Vallet-Regi M, Arcos D. Silicon substituted hydroxyapatites: a method to upgrade calcium phosphate based implants. J Mater Chem 2005;15:1509–16.
[12] Pietak AM, Reid JW, Stott MJ, Sayer M. Silicon substitution in the calcium phosphate bioceramics. Biomaterials 2007;28:4023–32.
[13] Patel N, Best SM, Bonfield W, Campus RF, Street RH. A comparative study on the in vivo behavior of hydroxyapatite and silicon substituted hydroxyapatite granules. J Mater Sci – Mater Med 2002;3:1199–206.
[14] Porter AE, Patel N, Skepper JN, Best SM, Bonfield W. Comparison of in vivo dissolution processes in hydroxyapatite and silicon-substituted hydroxyapatite bioceramics. Biomaterials 2003;24:4609–20.
[15] Vorndran E, Klammert U, Ewald A, Barralet JE, Gbureck U. Simultaneous immobilization of bioactives during 3D powder printing of bioceramic drug-release matrices. Adv Funct Mater 2010;20:1585–91.
[16] Inzana J, Olvera D, Fuller SM, Kelly JP, Graeve O, Schwarz EM, et al. 3D printing of composite calcium phosphate and collagen scaffolds for bone regeneration. Biomaterials 2014;35:4026–34.
[17] Arcos D, Rodríguez-Carvajal J, Vallet-Regí M. Silicon incorporation in hydroxylapatite obtained by controlled crystallization. Chem Mater 2004;16:2300–8.
[18] Azami M, Rabiee M, Moztarzadeh F. Glutaraldehyde crosslinked gelatin/hydroxyapatite nanocomposite scaffold, engineered via compound techniques. Polym Compos 2010;31:2112–20.
[19] Martínez-Vázquez FJ, Miranda P, Guiberteau F, Pajares A. Reinforcing bioceramic scaffolds with in situ synthesized ε-polycaprolactone coatings. J Biomed Mater Res A 2013;101:3551–9.
[20] Lozano D, Sánchez-Salcedo S, Portal-Núñez S, Vila M, López-Herradón A, Ardura JA, et al. Parathyroid hormone-related protein (107–111) improves the bone regeneration potential of gelatin-glutaraldehyde biopolymer-coated hydroxyapatite. Acta Biomater 2014;10:3307–16.
[21] Manzano M, Lozano D, Arcos D, Portal-Núñez S, la Orden CL, Esbrit P, et al. Comparison of the osteoblastic activity conferred on Si-doped hydroxyapatite scaffolds by different osteostatin coatings. Acta Biomater 2011;7:3555–62.
[22] Lozano D, Manzano M, Doadrio JC, Salinas AJ, Vallet-Regí M, Gómez-Barrena E, et al. Osteostatin-loaded bioceramics stimulate osteoblastic growth and differentiation. Acta Biomater 2010;6:797–803.
[23] Saiz E, Gremillard L, Menendez G, Miranda P, Gryn K, Tomsia AP. Preparation of porous hydroxyapatite scaffolds. Mater Sci Eng C 2007;27:546–50.
[24] Colilla M, Martinez-Carmona M, Sanchez-Salcedo S, Ruiz-Gonzalez ML, Gonzalez-Calbet JM, Vallet-Regi M. A novel zwitterionic bioceramic with dual antibacterial capability. J Mater Chem B 2014;2:5639–51.
[25] Cheng L, Zhang SM, Chen PP, Huang SL, Cao RR, Zhou W, et al. Fabrication and characterization of nano-hydroxyapatite/poly (D, L-lactide) composite porous scaffolds for human cartilage tissue engineering. Key Eng Mater 2006;309–311:943–8.
[26] Fowler BO. Infrared studies of apatites. I. Vibrational assignments for calcium, strontium, and barium hydroxyapatites utilizing isotopic substitution. Inorg Chem 1974;13:194–207.
[27] Chang BS, Lee CK, Hong KS, Youn HJ, Ryu HS, Chung SS, et al. Osteoconduction at porous hydroxyapatite with various pore configurations. Biomaterials 2000;21:1291–8.
[28] Boyan BD, Hummert TW, Dean DD, Schwartz Z. Role of material surfaces in regulating bone and cartilage cell response. Biomaterials 1996;17:137–46.
[29] Menzies KL, Jones L. The impact of contact angle on the biocompatibility of biomaterials. Optom Vis Sci 2010;87:387–99.
[30] Faucheux N, Schweiss R, Lützow K, Werner C, Groth T. Self-assembled monolayers with different terminating groups as model substrates for cell adhesion studies. Biomaterials 2004;25:2721–30.
[31] Dekker A, Reitsma K, Beugeling T, Bantjes A, Feijen J, van Aken WG. Adhesion of endothelial cells and adsorption of serum proteins on gas plasma-treated polytetrafluoroethylene. Biomaterials 1991;12:130–8.
[32] Miranda P, Pajares A, Saiz E, Tomsia AP, Guiberteau F. Fracture modes under uniaxial compression in hydroxyapatite scaffolds fabricated by robocasting. J Biomed Mater Res, Part A 2007;83A:646–55.
[33] Deville S, Saiz E, Tomsia AP. Freeze casting of hydroxyapatite scaffolds for bone tissue engineering. Biomaterials 2006;27:5480–9.
[34] Almirall A, Larrecq G, Delgado JA, Martínez S, Planell JA, Ginebra MP. Fabrication of low temperature macroporous hydroxyapatite scaffolds by foaming and hydrolysis of an alpha-TCP paste. Biomaterials 2004;25:3671–80.
[35] Del Real RP, Wolke JGC, Vallet-Regí M, Jansen JA. A new method to produce macropores in calcium phosphate cements. Biomaterials 2002;23:3673–80.
[36] Kawata M, Uchida H, Itatani K, Okada I, Koda S, Aizawa M. Development of porous ceramics with well-controlled porosities and pore sizes from apatite fibers and their evaluations. J Mater Sci – Mater Med 2004;15:817–23.
[37] Li W, Nooeaid P, Roether JA, Schubert DW, Boccaccini AR. Preparation and characterization of vancomycin releasing PHBV coated 45S5 Bioglass®-based glass–ceramic scaffolds for bone tissue engineering. J Eur Ceram Soc 2014;34:505–14.
[38] Milosevski M, Bossert J, Milosevski D, Gruevska N. Preparation and properties of dense and porous calcium phosphate. Ceram Int 1999;25:693–6.
[39] Ramay HRR, Zhang M. Biphasic calcium phosphate nanocomposite porous scaffolds for load-bearing bone tissue engineering. Biomaterials 2004;25:5171–80.
[40] Ramay HR, Zhang M. Preparation of porous hydroxyapatite scaffolds by combination of the gel-casting and polymer sponge methods. Biomaterials 2003;24:3293–302.
[41] Tian J, Tian J. Preparation of porous hydroxyapatite. J Mater Sci 2001;36:3061–6.
[42] Ioku K, Yanagisawa K, Yamasaki N, Kurosawa H, Shibuya K, Yokozeki H. Preparation and characterization of porous apatite ceramics coated with beta-tricalcium phosphate. Biomed Mater Eng 1993;3:137–45.
[43] Landi E, Celotti G, Logroscino G, Tampieri A. Carbonated hydroxyapatite as bone substitute. J Eur Ceram Soc 2003;23:2931–7.
[44] Liu D-M. Influence of porosity and pore size on the compressive strength of porous hydroxyapatite ceramic. Ceram Int 1997;23:135–9.
[45] Barralet JE, Grover L, Gaunt T, Wright AJ, Gibson IR. Preparation of macroporous calcium phosphate cement tissue engineering scaffold. Biomaterials 2002;23:3063–72.
[46] Pilliar R, Filiaggi M, Wells J, Grynpas M, Kandel R. Porous calcium polyphosphate scaffolds for bone substitute applications – in vitro characterization. Biomaterials 2001;22:963–72.
[47] Tancred D. A synthetic bone implant macroscopically identical to cancellous bone. Biomaterials 1998;19:2303–11.
[48] Chu T-MG, Orton DG, Hollister SJ, Feinberg SE, Halloran JW. Mechanical and in vivo performance of hydroxyapatite implants with controlled architectures. Biomaterials 2002;23:1283–93.
[49] Dong J, Kojima H, Uemura T, Kikuchi M, Tateishi T, Tanaka J. In vivo evaluation of a novel porous hydroxyapatite to sustain osteogenesis of transplanted bone marrow-derived osteoblastic cells. J Biomed Mater Res 2001;57:208–16.
[50] Landi E, Tampieri A, Celotti G, Langenati R, Sandri M, Sprio S. Nucleation of biomimetic apatite in synthetic body fluids: dense and porous scaffold development. Biomaterials 2005;26:2835–45.
[51] Miranda P, Pajares A, Saiz E, Tomsia AP, Guiberteau F. Mechanical properties of calcium phosphate scaffolds fabricated by robocasting. J Biomed Mater Res A 2008;85:218–27.
[52] Wang F. Structure and properties of bone-like-nanohydroxyapatite/gelatin/polyvinyl alcohol composites. Adv Biosci Biotechnol 2010;01:185–9.
[53] Bigi A, Panzavolta S, Roveri N. Hydroxyapatite–gelatin films: a structural and mechanical characterization. Biomaterials 1998;19:739–44.
[54] Hench LL, Jones JR, Institute of Materials Minerals. Biomaterials, Artificial Organs and Tissue Engineering. Cambridge: Woodhead Publishing; 2005.
[55] Peroglio M, Gremillard L, Gauthier C, Chazeau L, Verrier S, Alini M, et al. Mechanical properties and cytocompatibility of poly(ε-caprolactone)-infiltrated biphasic calcium phosphate scaffolds with bimodal pore distribution. Acta Biomater 2010;6:4369–79.
[56] Ko C-C, Oyen M, Fallgatter AM, Hu W-S. Effects of gelatin on mechanical properties of hydroxyapatite-gelatin nano-composites. MRS Proc 2011;898.0898–L08–01.
[57] Murugan R, Ramakrishna S. Development of nanocomposites for bone grafting. Compos Sci Technol 2005;65:2385–406.
[58] Cabañas MV, Peña J, Román J, Ramírez-Santillán C, Matesanz MC, Feito MJ, et al. Design of tunable protein-releasing nanoapatite/hydrogel scaffolds for hard tissue engineering. Mater Chem Phys 2014;144:409–17.
[59] Schäfer M, Schneider TR, Sheldrick GM. Crystal structure of vancomycin. Structure 1996;4:1509–15.
[60] Liu C, Xia Z, Czernuszka JT. Design and development of three-dimensional scaffolds for tissue engineering. Chem Eng Res Des 2007;85:1051–64.
[61] Costa P, Sousa Lobo JM. Modeling and comparison of dissolution profiles. Eur J Pharm Sci 2001;13:123–33.
[62] Cabañas MV, Peña J, Román J, Vallet-Regí M. Tailoring vancomycin release from beta-TCP/agarose scaffolds. Eur J Pharm Sci 2009;37:249–56.
[63] Keller TS. Predicting the compressive mechanical behavior of bone. J Biomech 1994;27:1159–68.

Please cite this article in press as: Martínez-Vázquez FJ et al. Fabrication of novel Si-doped hydroxyapatite/gelatine scaffolds by rapid prototyping for drug delivery and bone regeneration. Acta Biomater (2015), http://dx.doi.org/10.1016/j.actbio.2014.12.021